

## Synthesis and photophysical studies of phthalocyanine–gold nanoparticle conjugates

Nolwazi Nombona, Edith Antunes, Christian Litwinski and Tebello Nyokong\*

Received 19th June 2011, Accepted 26th August 2011

DOI: 10.1039/c1dt11151e

This work reports on the synthesis, characterization and photophysical studies of phthalocyanine–gold nanoparticle conjugates. The phthalocyanine complexes are: tris-(5-trifluoromethyl-2-mercaptopyridine)-2-(carboxy)phthalocyanine (**3**), 2,9,17,23-tetrakis-[(1, 6-hexanedithiol) phthalocyaninato]zinc(II) (**8**) and [8,15,22-tris-(naphtho)-2(amidoethanethiol) phthalocyanato] zinc(II) (**10**). The gold nanoparticles were characterized using transmission electron microscopy, X-ray diffraction, atomic force microscopy and UV-vis spectroscopy where the size was confirmed to be ~5 nm. The phthalocyanine Au nanoparticle conjugates showed lower fluorescence quantum yield values with similar fluorescence lifetimes compared to the free phthalocyanines. The Au nanoparticle conjugates of **3** and **10** also showed higher triplet quantum yields of 0.69 to 0.71, respectively. A lower triplet quantum yield was obtained for the conjugate compared to free phthalocyanine for complex **8**. The triplet lifetimes ranged from 70 to 92  $\mu$ s for the conjugates and from 110 to 304  $\mu$ s for unbound Pc complexes.

## Introduction

Photodynamic therapy (PDT) is a well known alternative for cancer treatment currently in clinical trials.<sup>1–4</sup> This therapy is based on the principle that upon irradiation, a photosensitiser will get excited and transfer its energy to the surrounding oxygen generating singlet oxygen,<sup>5,6</sup> which causes cellular damage to surrounding cancerous cells *via* necrosis or apoptosis.<sup>7–9</sup> Due to the poor drainage in tumour cells, the photosensitiser efficiently accumulates in tumour cells, making PDT a more efficient method for cancer treatment.<sup>10</sup>

Nanotechnology has become a thriving area of research that has significantly transformed the health care system by fighting deadly diseases more competently.<sup>11,12</sup> The properties of nanoparticles differ from the bulk and individual atoms they are comprised of.<sup>13–17</sup>

Ligands such as phthalocyanines can be attached to nanoparticles in order to improve their properties with regards to better drug specificity.<sup>18</sup> Phthalocyanines conjugated to nanoparticles have demonstrated improved necrosis and/or apoptosis.<sup>19</sup> The gratifying toxicity profile of gold and platinum nanoparticles makes them favourable for medicinal application.<sup>20,21</sup>

Conjugates of phthalocyanines and Au nanoparticles (AuNPs) have been reported for drug delivery applications.<sup>19,22,23</sup> The phthalocyanine complexes employed were either disulfide derivatives or those substituted with one SH terminal group. Gold nanoparticles decreased the fluorescence lifetime of the Pc molecule,

suggesting energy transfer from the Pc to the AuNP, though the phase transfer agent (tetraoctylammonium bromide, TOABr) is also known to decrease the lifetimes of free Pcs.<sup>22</sup> Energy transfer from the photoexcited phthalocyanines to the gold nanoparticles occurs in the picosecond time scale of ~3 ps.<sup>24</sup> In another study,<sup>25</sup> gold nanoparticles were found not to quench the fluorescence of cobalt tetraminophthalocyanine, whereas silver nanoparticles did.

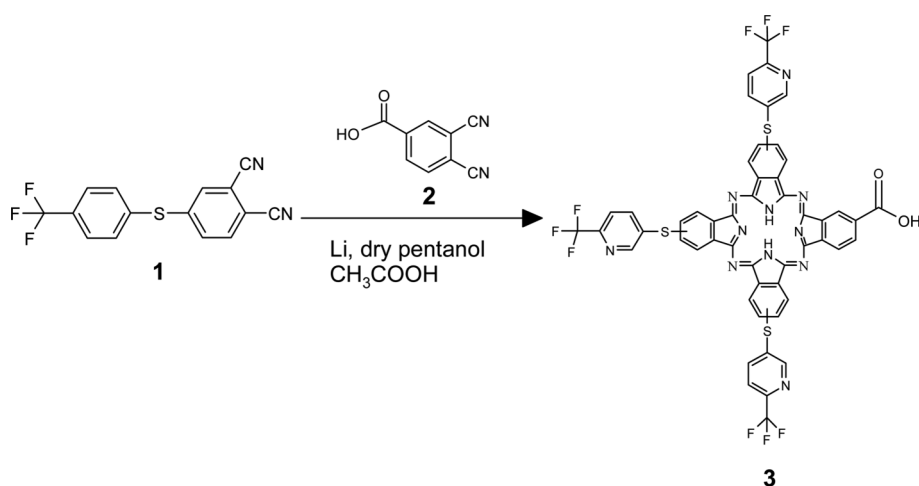
Thus it is clear from the literature that the fluorescence behaviour of phthalocyanines alone or in the presence of AuNPs depends on the nature of the macrocycle. In this work, we compare the effects of AuNP on the photophysical behaviour of phthalocyanines containing SR groups (**3**), four SH groups (**8**) or one SH group (**10**), see Schemes 1 to 3 for structures. The rest of the substituents (for **3** and **10**) were chosen to enhance solubility of the Pc complexes. Both unmetallated and Zn phthalocyanine complexes are employed. Ligand exchange was used as a method for phthalocyanine attachment on the nanoparticles. The phthalocyanine complexes employed are: 9,16,23-tris-(5-trifluoromethyl-2-mercaptopyridine)-2-(carboxy)phthalocyanine (**3**, containing sulfur bridges), 2,9,17,23-tetrakis-[(1, 6-hexanedithiol)phthalocyaninato]zinc(II) (**8**) and [8,15,22-tris-(naphtho)-2(amidoethanethiol)phthalocyanato]zinc(II), containing a terminal SH group (**10**).

## Results and Discussion

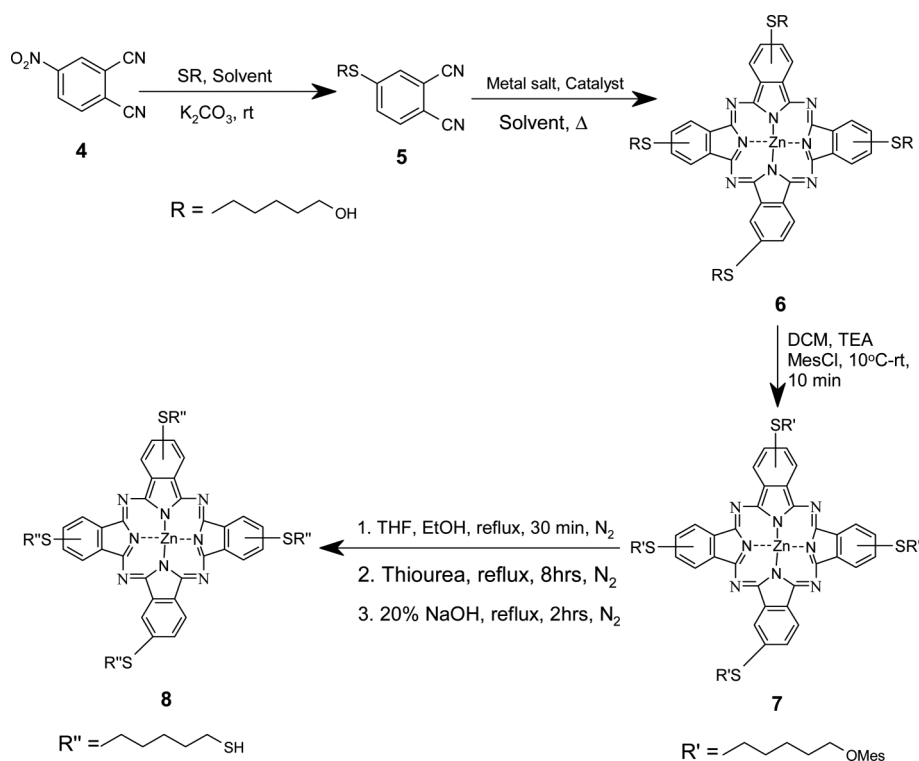
## Synthesis and characterization

**Phthalocyanine complexes.** The syntheses and characterization of complex **9** (Scheme 3) has been previously described.<sup>26</sup>

Department of Chemistry, Rhodes University, Grahamstown, 6140, South Africa. E-mail: t.nyokong@ru.ac.za; Fax: +27 46 622 5109



**Scheme 1** Synthetic pathway of 9,16,23-tris-(5-trifluoromethyl-2-mercaptopyridine)-2-(carboxy)phthalocyanine (**3**).

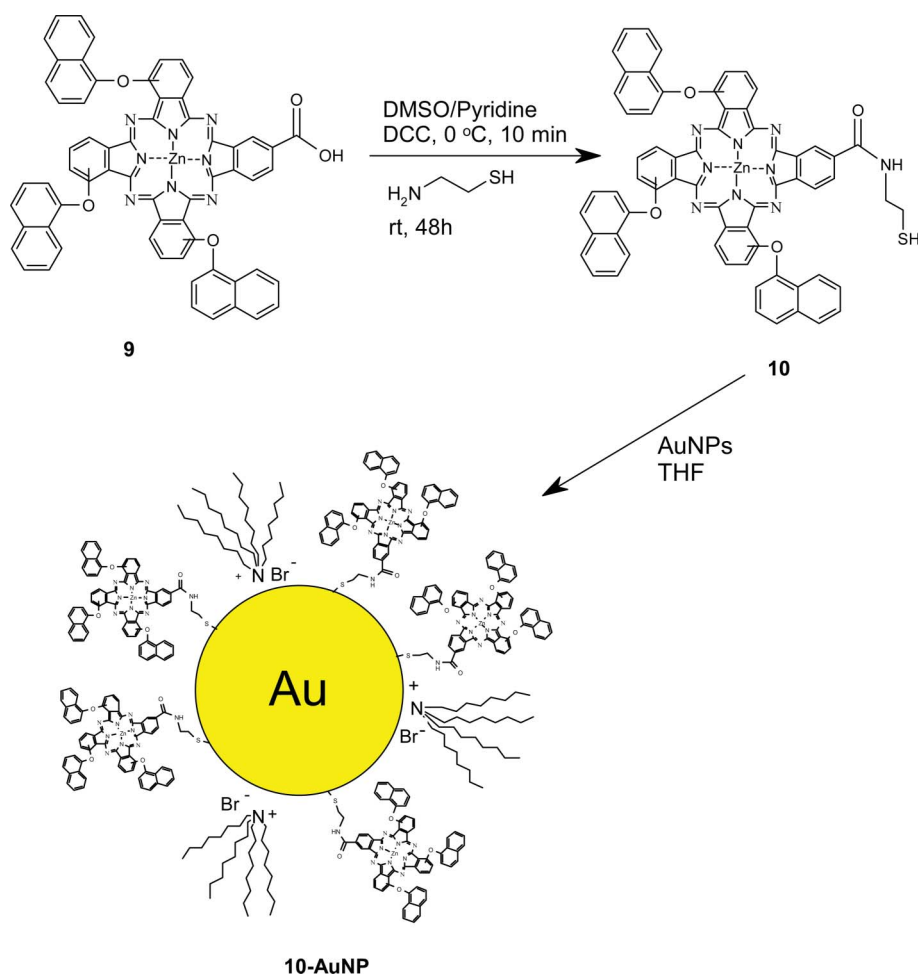


**Scheme 2** Synthetic route of 4-(6-mercaptohexan-1-ol) phthalonitrile (**5**) and 2,9,17,23-tetrakis-[(1, 6-hexanedithiol)phthalocyaninato]zinc(II) (**8**).

Compounds **1**, **2** and **4** were synthesized according to literature<sup>27–29</sup> and the synthetic strategy used for the synthesis of **3** (Scheme 1) was similar to that reported for the pyridyloxy derivative.<sup>30</sup> The synthesis of unsymmetrical phthalocyanines is complicated compared to symmetrically substituted Pcs as they often require extensive purification methods to obtain the desired product. To increase the product yield for complex **3**, compounds **1** and **2** were ground together. The powder was added to a refluxing mixture of dry pentanol containing dissolved lithium. A relatively good yield for the unsymmetrical phthalocyanine (**3**) was obtained (13%) after continuous washing in hot methanol and purification by column chromatography. The different lipophilicities of **1** and **2** assisted in the purification of **3** from by-products due to different

silica-binding properties in the solvent mixture employed. The phthalocyanine showed partial solubility in most organic solvents including dimethylsulfoxide (DMSO), dichloromethane (DCM), methanol, acetone and toluene. However it showed good solubility in chloroform dimethylformamide (DMF) and tetrahydrofuran (THF).

Scheme 2 shows the chemical structure and synthetic route of compound **8**. The synthesis of complex **8** starts with the synthesis of **5**. The base catalyzed nucleophilic substitution of the nitro functional group on phthalonitrile **4** with mercaptohexanol was achieved in dry DMSO at room temperature under inert nitrogen atmosphere with good yields obtained for phthalonitrile **5**.<sup>27–29</sup> The conversion of **5** into the corresponding hydroxyl substituted



**Scheme 3** Synthetic route of [8,15,22-tris-(naphtho)-2-(amidoethanethiol) phthalocyanato] zinc(II) (**10**) and **10-AuNP** conjugate.

zinc phthalocyanine (**6**) was accomplished in pentanol in the presence of a catalyst and zinc acetate. The terminal hydroxyl groups on complex **6** were converted into their mesylate counterparts using triethanolamine (TEA) followed by the addition of methanesulfonyl chloride at low temperature under standard reaction conditions to give the substituted phthalocyanine **7**. Finally, the terminal thiol functional group was obtained by refluxing thiourea, under an inert atmosphere in the absence of light, in a previously degassed THF/ethanol solvent mixture. The resultant product was then hydrolysed using 20% NaOH (also previously degassed). The inert atmosphere inhibits the formation of disulfides *via* aerobic oxidations and ensures the formation of complex **8** at a relatively low yield.

Bulky naphthol non-peripheral substituents were purposely chosen for complex **9** to reduce the typical aggregation of the planar macrocyclic system and to allow for simple determination of the photophysical properties of the complex in the monomeric form. Complex **9** was covalently linked to cysteamine in the presence of an amide coupling agent dicyclohexylcarbodiimide (DCC) in a DMSO/pyridine mixture to form complex **10**. DCC reacts with the carboxylic acid to form the O-acylisourea anhydride intermediate. This intermediate is more reactive than the resonance stabilised carboxylic centre and can directly react with the amine to yield complex **10**. The formation of possible by-

products was diminished by reacting **9** with DCC in the presence of a base (pyridine) at 0 °C prior to the addition of cysteamine. Purification of the complex was achieved using BioBeads with THF as the eluent.

Characterization of complexes **3**, **8** and **10** were achieved using infra-red (IR), ultraviolet-visible (UV-Vis), matrix-assisted laser desorption/ionization-time of flight (MALDI-TOF) mass spectra and proton nuclear magnetic resonance (<sup>1</sup>H NMR) spectroscopies as well as elemental analyses.

The absence of the sharp C≡N vibration (~2230 cm<sup>-1</sup>) for compounds **1**, **2**, **4** and **5** in the IR spectra of **3** and **8** confirmed phthalonitrile cyclisation. For **3** the typical N–H band at 1079 cm<sup>-1</sup> further confirmed unmetallated Pc formation and the IR spectroscopy data for complex **10** confirmed amide bond formation with a peak observed at 1693 cm<sup>-1</sup>.

The <sup>1</sup>H NMR spectrum for complex **3** showed 21 aromatic protons between 6.35 to 8.21 ppm. MALDI-TOF MS further confirmed the formation of complex (**3**) with a molecular ion peak observed at 1090 amu.

Complex **8** was found to be pure by <sup>1</sup>H NMR. Aromatic protons were observed between 6.97 and 7.70 ppm integrating for 12 and CH<sub>2</sub> protons were between 4.22 and 1.24 ppm, integrating for 48 protons, in total, as expected. The mass spectra of the complex showed a molecular ion peak at 1170.56 amu.

**Table 1** UV-Vis spectral parameters of phthalocyanines and phthalocyanine-AuNP conjugates in chloroform, unless otherwise stated

Pc	$^a\lambda_{\text{abs}}/\text{nm}$	$^a\lambda_{\text{ems}}/\text{nm}$	$^a\lambda_{\text{exc}}/\text{nm}$	$\Phi_{\text{F}}$	$^b\Phi_{\text{T}}$	$\tau_{\text{T}}/\mu\text{s}$
<b>3</b>	667, 703	708	669, 701	0.04	0.68	110
<b>3-AuNP</b>	667, 704	709	670, 703	0.02	0.71	92
<b>8</b>	704	716	705	0.15	0.75	304
<b>8-AuNP</b>	698	716	708	0.07	0.69	87
<b>9</b>	691	708	697	0.1	0.62	240
<b>10</b>	692	704	696	0.05	0.63	140
<b>10-AuNP</b>	689	701	694	0.04	0.71	70

$^a\lambda_{\text{abs}}$  = Q band absorption maximum,  $\lambda_{\text{ems}}$  = Q band emission maximum,  $\lambda_{\text{exc}}$  = Q band excitation maximum.  $^b\Phi_{\text{T}}$  = values were obtained in DMF.

For complex **10**,  $^1\text{H}$  NMR showed aromatic protons between 6.72 and 8.20 ppm integrating for 34 protons and  $\text{CH}_2$  protons being observed between 0.82 and 1.50 integrating for 4 protons as expected. MALDI-TOF MS further confirmed the formation of complex **10** with a mass peak observed at 1108.24 amu.

The UV-vis spectrum of **3** in chloroform is shown in Fig. 1A (spectrum i). A split Q-band was observed for **3** with maxima at 667 and 703 nm, Table 1. The splitting of the Q band is typical for metal-free Pc and is caused by reduced symmetry of the molecule. The B band was observed at 340 nm for **3**.

Complex **3** is aggregated in DMF and DMSO, and less aggregated in chloroform. Thus chloroform was chosen as a solvent to allow for comparison of **3** with other complexes (**8** and **10**, which are not aggregated in chloroform). For complex **3** in chloroform, there is a slight broadening of the absorption bands between 550 and 650 nm, typical of aggregation in phthalocyanine complexes.<sup>31</sup> However, there was no observed disaggregation on addition of Triton X or chromophore EL as surfactants. Complex **3** obeys Beer's law at concentrations lower than  $1.5 \times 10^{-6}$  M in chloroform. The absorbance spectra of complex **8** showed slight aggregation in DMSO and DMF with no aggregation observed in chloroform, Fig. 1B, with Q band maxima at 704 nm in chloroform.

Fig. 1C shows that complexes **9** and **10** display similar spectra in terms of Q band maxima, showing the presence of one SH band does not affect the spectra. MPc complexes containing sulfur groups are usually red-shifted. Complex **10** shows a split in the Q band which could be due to the loss of symmetry as a result of unsymmetric substitution (which should also affect **3** and **9**) or due to protonation of the aza nitrogens caused by the acidic chloroform.<sup>32</sup> The protonation would be substituent specific since it depends on the basicity of the ring, hence we suggest that the split in the Q band is due to loss of symmetry as a result of unsymmetrical protonation of the inner nitrogen atom.

**AuNPs and Pc-AuNP conjugates.** Phthalocyanine-functionalised gold nanoparticles were synthesized using a ligand exchange process, where the loosely bound TOABr ligands were partially exchanged by Pcs that bind covalently to the nanoparticle surface. The phthalocyanine complexes were most likely attached to the AuNPs surface *via* Au-S bond due to the sulfur groups on the periphery of the phthalocyanine ring, for complexes **3**, **8** and **10**. A schematic representation of the conjugation of **10** with the TOABr-AuNP is shown in Scheme 3. For complex **10** containing one thiol group, the arrangement

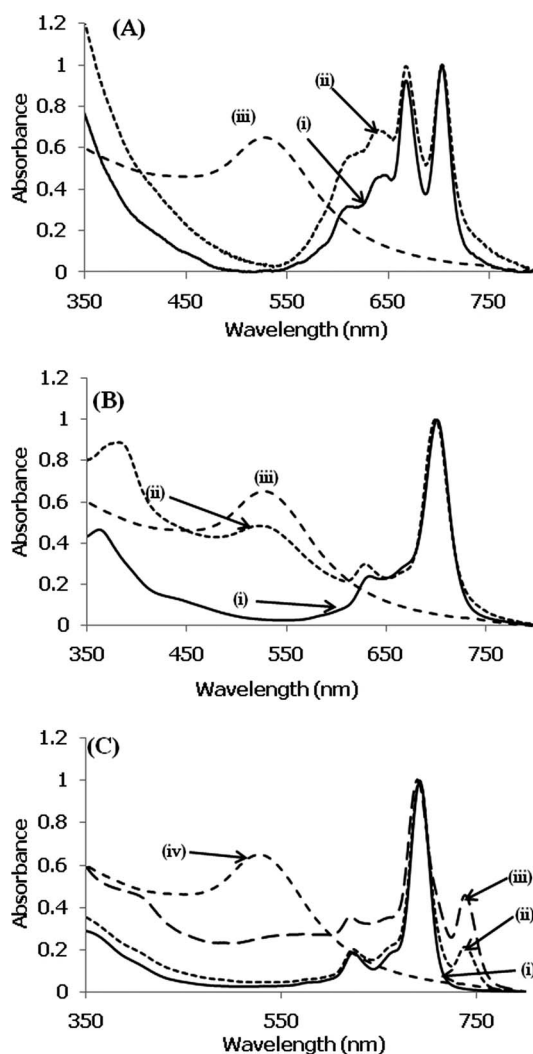


**Fig. 1** Absorption spectra (concentration =  $\sim 1 \times 10^{-5}$  M) of (A) compound **3** (i), **3-AuNP** (ii) and **TOABr-AuNP** (iii), (B) compound **8** (i), **8-AuNP** (ii) and **TOABr-AuNP** (iii), (C) compound **9** (i), **10** (ii), **10-AuNP** (iii) and **TOABr-AuNP** (iv) in chloroform.

of the phthalocyanines will be by linkage with this one group, resulting in a perpendicular arrangement shown in Scheme 3. For complexes **3** and **8**, it is possible that one or more of the SR or SH groups are attached.

The Au nanoparticles were characterised using UV-Vis and X-ray diffraction (XRD) spectroscopies as well as atomic force microscopy (AFM) and transmission electron microscopy (TEM). To determine the size of the gold nanoparticles and the Pc-AuNP conjugates, XRD technique was employed. The Debye-Scherrer equation<sup>33</sup> (eqn (1)) was used to calculate the size of the gold nanoparticles and Pc conjugates.

$$d(\text{\AA}) = \frac{k\lambda}{\beta \cos\theta} \quad (1)$$

where  $k$  is an empirical constant equal to 0.9,  $\lambda$  is the wavelength of the X-ray source, (1.5405 Å),  $\beta$  is the full width at half maximum of the diffraction peak, and  $\theta$  is the angular position of the peak. Fig. 2 shows the XRD pattern for the AuNPs and the corresponding TOABr pattern employed in this work, the average

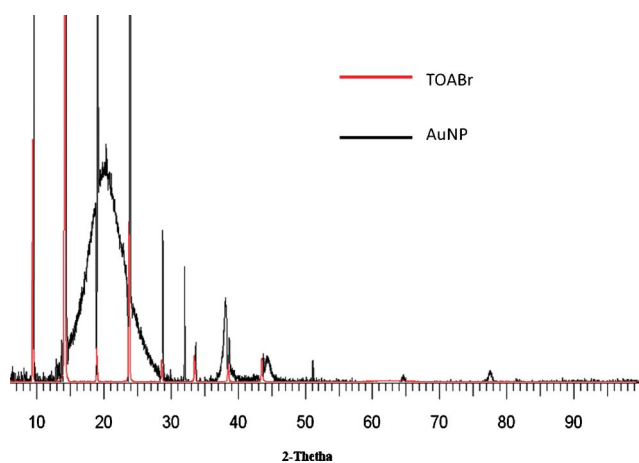


Fig. 2 XRD of TOABr-AuNP and TOABr.

size for the AuNPs was calculated to be 5.37 nm when the peak at  $64.63^\circ$  corresponding to gold was fitted. This size was further confirmed by atomic force microscopy where the average size of the nanoparticles ranged between 3.5 and 4.5 nm. Fig. 3 shows the size distribution of the gold nanoparticles as determined by AFM.

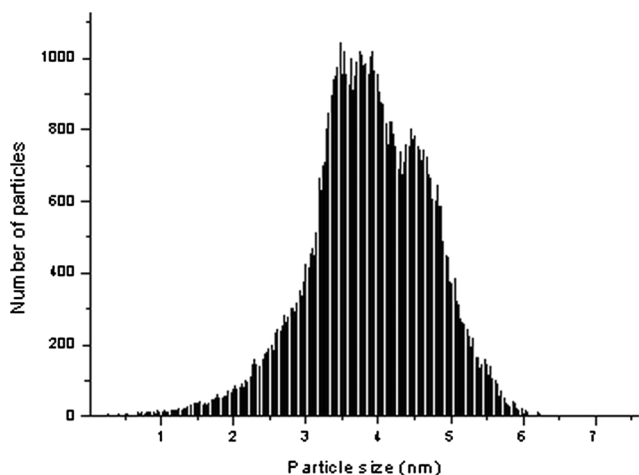


Fig. 3 Size distribution histogram (from AFM) of synthesized gold nanoparticles.

Fig. 4a shows the TEM image of the TOABr-AuNP and Fig. 4b and 4c show the TEM images of the **8-AuNP** and **10-AuNP**, respectively. Fig. 4a shows the AuNPs as spheres with different sizes dispersed in a disorderly manner, these are seen as dark spots on the TEM image.

On conjugation with Pc complexes TEM images (using **8-AuNP** and **10-AuNP** as examples) show a highly ordered arrangement, Fig. 4b and 4c. The size of the nanoparticles determined from the TEM image was found to range between 5.97–7.87 nm. The size of AuNPs (~5 nm) determined using XRD is expected to be more reliable, unlike TEM which is an estimation due to partial aggregation. The size determined using AFM is closer to that determined using XRD.

The surface plasmon resonance (SPR) band for AuNP absorption was determined from UV-vis spectrum to be 518 nm

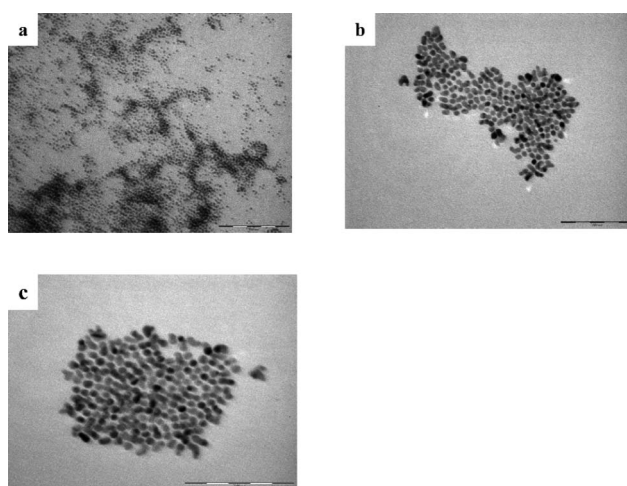


Fig. 4 TEM images of TOABr-AuNP (a), **8-AuNP** (b) and **10-AuNP** (c).

(Fig. 1). This is consistent with the reported SPR peak for gold nanoparticles of sizes less than 50 nm.<sup>16,34</sup>

The UV-vis spectra of the Pc-AuNP conjugates are shown in Fig. 1 for **3-AuNP**, **8-AuNP** and **10-AuNP** and together with their unconjugated phthalocyanine derivatives. It is known that the absorption spectrum of the Pc-AuNP shows a broadening of the phthalocyanine Q-band absorption, this was attributed to a tight packing of the phthalocyanines on the gold.<sup>24</sup> In Fig. 1A for **3-AuNP** this broadening is observed, in addition there is a small blue shift since the SR groups are now engaged with the AuNPs reducing their electron donating abilities. Similarly, a slight blue shift is observed for **8-AuNP** in Fig. 1B and for **10-AuNP** in Fig. 1C. For **10-AuNP**, there is an increase in a split in the Q band, which suggests that the splitting due to loss of symmetry is enhanced by attachment of AuNPs. A closer look at Fig. 1B for **8-AuNP**, shows the SPR peak in the conjugate to be larger than for **3-AuNP** or **10-AuNP**, suggesting more coordinated AuNPs, in the latter two conjugates. The diminished and broad surface plasmon band has been found to be indicative of surface complexation; hence the SPR band serves as a probe to monitor the interaction between AuNPs with surface bound molecules.<sup>35</sup>

## Photophysical properties

**Fluorescence spectra, quantum yields and lifetimes.** Fig. 5 shows the absorption, emission and excitation spectra of **3**

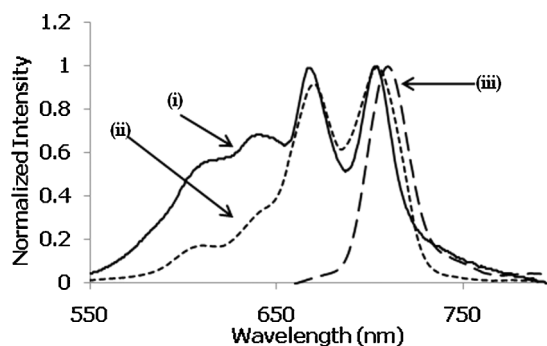


Fig. 5 Absorption (i), excitation (ii) and emission (iii) spectra of **3**.

in chloroform. The excitation spectra showed the typical split Q-band at the same wavelength positions as the absorption spectra. The lack of agreement between excitation and absorption spectra, is due to the absorption of the latter with broad bands between 600 and 650 nm due to aggregates. These bands are not observed in the excitation spectra since aggregated species do not fluoresce. The observation of a single band in the emission spectrum is typical of low symmetry phthalocyanines such as unmetallated ones.<sup>36</sup> Fluorescence quantum yield of **3** was determined to be 0.04, Table 1.

The absorption, emission and excitation spectra of **3-AuNP** in chloroform showed similar behaviour to complex **3** alone. The nearness of the absorption Q band wavelength (especially the low energy component) with the excitation Q band wavelength (for **3** or **3-AuNP**) implies that the nuclear configurations of the ground and excited states are similar and not affected by excitation, Table 1. The fluorescence quantum yield of **3** was slightly higher than for **3-AuNP** (Table 1) confirming that the presence of AuNPs lowers the  $\Phi_F$ , and that AuNPs quench fluorescence as has been reported before,<sup>24</sup> contrary to when cobalt tetraamino phthalocyanine interacts with AuNPs.<sup>25</sup> Comparing **9** and **10** shows that the presence of the thiol group in complex **10** lowered the quantum yield value from 0.1 (**9**) to 0.05 for **10**, however the quantum yield value for **10-AuNP** was similar to that of the free phthalocyanine. The conjugation of AuNPs did not have a significant effect on the  $\Phi_F$  value for **10-AuNP**.

The fluorescence emission spectra were mirror images of the absorption spectra for the metalated complexes. A decrease in the fluorescence quantum yield of **8-AuNP** compared to **8** was rather significant suggesting that the presence of the AuNPs strongly quenches fluorescence as was also the case for **3-AuNP**.

Typically, Pcs in close proximity with AuNPs experience emission quenching which can originate either from enhanced intersystem crossing due to the heavy atom effect or through direct energy transfer from the Pc to the AuNPs. This energy transfer is called surface energy transfer (SET) as the photoexcited Pc transfers its energy to the AuNP, upon relaxation back to the ground state. This phenomenon generally occurs for gold nanoparticles with small diameters<sup>37</sup> and that are larger than for Foster resonance energy transfer (FRET).<sup>38</sup> It is possible that the slight aggregation observed for phthalocyanines when conjugated to AuNPs can result in self-quenching decreasing the fluorescence quantum yields further.

Even though both the free and bound Pc were reported to have a double exponential function,<sup>22</sup> time-resolved fluorescence measurements for complex **3** indicate a mono-exponential decay (Fig. 6, Table 2), with fluorescence lifetimes ( $\tau_{F1}$ ) of 2.5 ns indicating that there is only one species in the solution. Complex **3-AuNP** showed a bi-exponential decay where the first component (with  $\tau_{F1}$  of 2.6) may be due to the presence of free phthalocyanines and the second component (with  $\tau_{F2}$  of 1.1 ns, Table 2) is due to derivatives conjugated to the nanoparticles. **10-AuNP** also showed bi-exponential decay with  $\tau_{F1}$  = 2.5 ns, and  $\tau_{F2}$  = 0.8 ns, Table 2. The second components for **3-AuNP** and **10-AuNP** were short-lived with low abundance. Complex **8-AuNP**, however, showed a mono-exponential decay suggesting that the phthalocyanines attached on the gold surface are highly quenched to the point where they are not fluorescent.

**Table 2** UV-Vis spectral parameters of phthalocyanines and phthalocyanine-AuNP conjugates in chloroform

Pc	$\tau_{F1}$ /ns	Relative amplitude	$\tau_{F2}$ /ns	Relative amplitude
<b>3</b>	2.5	1	—	—
<b>3-AuNP</b>	2.6	0.7	1.1	0.3
<b>8</b>	2.5	1	—	—
<b>8-AuNP</b>	2.5	1	—	—
<b>9</b>	4.5	1	—	—
<b>10</b>	2.7	1	—	—
<b>10-AuNP</b>	2.5	0.8	0.8	0.2

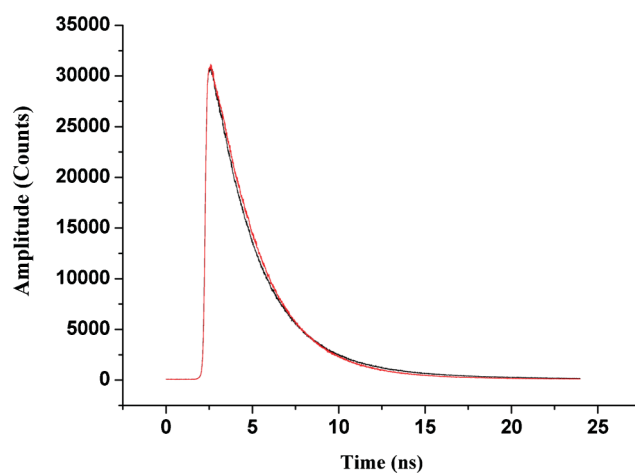


**Fig. 6** Fluorescence decay curve of complex **3** (red) and **3-AuNP** (black) in chloroform.

### Triplet quantum yields and lifetimes

The triplet quantum yield ( $\Phi_T$ ) values could not be determined in  $\text{CHCl}_3$  due to the lack of standard in this solvent, hence DMF was employed for these studies. Triplet quantum yields and lifetimes of the phthalocyanines and the conjugates were determined using laser flash photolysis. The triplet decay curves (figure not shown) of all complexes in DMF obeyed second order kinetics. This is typical of Pc complexes at high concentrations ( $>1 \times 10^{-5}$  M) due to the triplet-triplet recombination.<sup>25</sup> The concentrations employed in this work were in this range; hence triplet-triplet recombination is expected. Intersystem crossing to the triplet state and fluorescence are competing deactivating processes for a molecule in the excited singlet state. Therefore their values are complementary. Table 1 show high triplet quantum yield ( $\Phi_T$ ) values for the conjugates of **3** or **10** with AuNPs: 0.71 (for both **3-AuNP** and **10-AuNP**) in DMF compared to the free phthalocyanines where the  $\Phi_T$  values are 0.68 for **3** and 0.63 for **10**. This is due to the presence of the AuNPs that encourage intersystem crossing due to the heavy atom effect. For complex **8** containing four thiol groups, there is a surprising decrease in  $\Phi_T$  value in the presence of AuNPs. This could be due to the slight aggregation of **8** in DMF which was discussed above.

All the conjugates showed a decrease in triplet lifetimes in the conjugates compared to free phthalocyanines. The speedy deactivation of the triplet state for the conjugates may be explained by the heavy atom effect.

## Experimental section

### Materials

Chloroform (CHCl<sub>3</sub>), dimethyl sulfoxide (DMSO), tetrahydrofuran (THF) dimethylformamide (DMF), dichloromethane (DCM), methanol (MeOH), ethanol (EtOH), toluene, glacial acetic acid, acetone, pentanol, pyridine, hydrochloric acid, sodium hydroxide and sodium borohydride (95%) were purchased from SAARCHEM. Tetraoctylammonium bromide (TOABr) (98%), gold(III) chloride trihydrate (99.9%), dicyclohexylcarbodiimide (DCC) (99%), cysteamine hydrochloride, magnesium sulphate, methanesulfonylchloride, thiourea, triethanolamine (TEA), 6-mercaptohexan-1-ol and lithium metal were purchased from Sigma-Aldrich. Silica gel for column chromatography was purchased from Merck. Phthalonitriles **1**, **2** and **4** were synthesized as reported in the literature.<sup>27–29</sup> Tetraoctylammonium bromide gold nanoparticles (TOABr-AuNP) were synthesised according to literature.<sup>24,39</sup> The sizes of AuNPs were confirmed by atomic force microscopy, transmission electron microscopy and X-ray diffraction. Column chromatography was performed on silica gel 60 (0.04–0.063 mm) or on Bio-beads S-X1 200–400 mesh purchased from BioRad.

### Equipment

Ground state electronic absorption spectra were performed on a Shimadzu UV-2550 spectrophotometer; Infra-red spectra on a Perkin Elmer Spectrum 100 FT-IR Spectrometer and <sup>1</sup>H nuclear magnetic resonance signals on a Bruker AMX 400 MHz NMR spectrometer or with a Bruker AMX 600 MHz NMR spectrometer. Elemental analysis was done using a Vario-Elementar Microcube ELIII. Mass spectral data were collected with a Bruker AutoFLEX III Smartbeam TOF/TOF Mass spectrometer. The instrument was operated in positive ion mode using a *m/z* range of 400–3000 amu. The voltages of the ion sources were set at 19 and 16.7 kV for ion sources 1 and 2 respectively, while the lens was set at 8.50 kV. The reflector 1 and 2 voltages were set at 21 and 9.7 kV respectively. The spectra were acquired using dithranol as the MALDI matrix, using a 337 nm nitrogen laser. Transmission electron microscope (TEM) images were obtained using a JEOL JEM 1210 transmission electron microscope at 100 kV accelerating voltage. X-ray powder diffraction patterns were recorded on a Bruker D8 Discover equipped with a LynxEye detector, using Cu-K $\alpha$  radiation ( $\lambda = 1.5405 \text{ \AA}$ , nickel filter). Data were collected in the range from  $2\theta = 5^\circ$  to  $65^\circ$ , scanning at  $1^\circ \text{ min}^{-1}$  with a filter time-constant of 2.5 s per step and a slit width of 6.0 mm. Samples were placed on a zero background silicon wafer slide. The X-ray diffraction data were treated using Eva (evaluation curve fitting) software. Baseline correction was performed on each diffraction pattern. Atomic force microscopy (AFM) images were recorded in the non-contact mode in air with a CP-11 Scanning Probe Microscope from Veeco Instruments (Carl Zeiss, South Africa) at a scan rate of 1 Hz. The images were obtained using a spring constant range of 20–80 N m<sup>-1</sup>, and resonant frequency range of 217–276 Hz.

Fluorescence excitation and emission spectra were recorded on a Varian Eclipse fluorescence spectrofluorimeter. Fluorescence lifetimes were measured using a time correlated single photon counting setup (TCSPC) (FluoTime 200, Picoquant GmbH)

with a diode laser (LDH-P-670 with PDL 800-B, Picoquant GmbH, 670 nm, 20 MHz repetition rate, 44 ps pulse width). Fluorescence was detected under the magic angle with a peltier cooled photomultiplier tube (PMT) (PMA-C 192-N-M, Picoquant) and integrated electronics (PicoHarp 300E, Picoquant GmbH). A monochromator with a spectral width of about 8 nm was used to select the required emission wavelength band. The response function of the system, which was measured with a scattering Ludox solution (DuPont), had a full width at half-maximum (FWHM) of 300 ps. All luminescence decay curves were measured at the maximum of the emission peak and lifetimes were obtained by deconvolution of the decay curves using the FluorFit Software program (PicoQuant GmbH, Germany). The support plane approach<sup>40</sup> was used to estimate the errors of the decay times.

A laser flash photolysis system was used for the determination of triplet decay kinetics. The excitation pulses were produced by a Quanta-Ray Nd:YAG laser (1.5 J/9 ns), pumping a Lambda Physik FL 3002 dye laser (Pyridin 1 in methanol). The analyzing beam source was from a Thermo Oriel 66902 xenon arc lamp, and a Kratos Lis Projekte MLIS-X3 photomultiplier tube was used as the detector. Signals were recorded with a two-channel, 300 MHz digital real time oscilloscope (Tektronix TDS 3032C); the kinetic curves were averaged over 256 laser pulses. Triplet lifetimes were determined by exponential fitting of the kinetic curves using OriginPro 8 software.

### Synthesis

Syntheses of [8,15,22-tris-(naphtho)-2-(carboxy)phthalocyanato] zinc(II) (**9**) has been reported.<sup>26</sup>

**[9,16,23-Tris-(5-trifluoromethyl-2-mercaptopyridine)-2-(carboxy)phthalocyanine] (3, Scheme 1).** Using a mortar and pestle, 0.109 g (3 eq.) of **1** and 0.0204 g (1 eq.) of **2** were mixed and ground, and the powder was added in a round bottom flask containing a refluxing solution of dry pentanol (5 mL) with dissolved lithium (0.8 mmol). The reaction was stirred under reflux in an argon atmosphere at 140 °C for 2 h. Thereafter the reaction mixture was left to cool to room temperature. Glacial acetic acid (20 mL) was added and the precipitate of the crude complex **3** was centrifuged and washed with water. The purification of the product was carried out by repetitive washing in hot methanol; the product was thereafter dissolved in chloroform and column chromatography was carried out using a chloroform/DMF (9 : 1) mixture as the eluent. Multiple fractions were collected with the second fraction being the desired product. The product obtained was highly aggregated in numerous solvents including THF and DMSO, but less aggregated in chloroform. Yield: ~13%. UV-vis (CHCl<sub>3</sub>):  $\lambda_{\text{max}}$  nm (log  $\epsilon$ ): 699 (4.34), 664 (4.31), 635 (4.03), 603 (3.86), 340 (4.27). IR  $\nu_{\text{max}}$ /cm<sup>-1</sup>: 1595 (C–O coupled to O–H), 1323 (Aryl NH), 742 (C–S). Calc. for: C<sub>51</sub>H<sub>24</sub>N<sub>11</sub>S<sub>5</sub>O<sub>2</sub>F<sub>9</sub>: C, 60.80; H, 4.51; N, 9.45; S, 8.12%; found C, 60.40; H, 3.96; N, 9.42; S, 8.60%. <sup>1</sup>H NMR (CDCl<sub>3</sub>):  $\delta$ , ppm 8.21–6.35 (21H, m, Ar–H), (1H, s, OH) not observed, (2H, s, Pc–H) not observed. MALDI-TOF-MS *m/z* Calc: 1089.98; found [M]<sup>-</sup>: 1090.20

**4-(6-Mercaptohexan-1-ol) phthalonitrile (5, Scheme 2).** 6-Mercaptohexan-1-ol (1.48 mL, 11.22 mmol) and 4-nitrophthalonitrile (**4**) (1.68 g, 9.35 mmol) were dissolved

in DMSO (80 mL) under a stream of nitrogen and the mixture stirred at room temperature for 15 min. Thereafter, finely ground  $K_2CO_3$  (2.11 g, 15.31 mmol) was added portion wise over a period of 4 h and the reaction mixture left to stir for a further 24 h at room temperature. The mixture was then added to water (150 mL) and stirred for 30 min. The resulting precipitate was filtered off, thoroughly washed with diethyl ether and acetone, dried and recrystallized from ethanol. Yield: 90%. IR [(KBr)  $\nu_{max}/cm^{-1}$ ]: 3007 (C–H), 2230 (C≡N), 1668, 1583 (C=C), 1437, 1408, 1387 (C–H) 884, 666 (C–S–C).  $^1H$  NMR (600 MHz, DMSO- $d_6$ ):  $\delta$ , ppm: 7.65 (d, 1H, Ar–H), 7.57 (d, 1H, Ar–H), 7.50 (dd, 1H, Ar–H), 3.65 (t, 2H, O–CH<sub>2</sub>), 3.03 (t, 2H, S–CH<sub>2</sub>), 1.75 (m, 2H, CH<sub>2</sub>), 1.61–1.43 (m, 6H, CH<sub>2</sub>).

**[2,9,17,23-Tetrakis-(1,6-hexanedithiol)phthalocyaninato] zinc(II) (8, Scheme 2).** The synthetic route followed for the synthesis of complex **8** was the same as described by Chambrier *et al.*<sup>41</sup> Firstly, complex **6** was prepared by refluxing a mixture of anhydrous zinc(II) acetate (0.51 g, 2.8 mmol), 4-(6-mercaptohexan-1-ol)phthalonitrile (**5**) (0.5 g, 1.6 mmol), DBU (0.55 mL, 4 mmol) and pentanol (15 mL) at 160 °C for 5 h. The formed complex **6** (111 mg) was then dissolved in dry DCM (20 mL) in the presence of dry TEA (10 eq. 0.92 mmol). Methanesulfonyl chloride (10 eq. 0.92 mmol) was added to the solution with cooling to 10 °C. The solution was then stirred and allowed to warm to room temperature (10 min). The product in DCM was then washed with water, dried using  $MgSO_4$ , filtered and the DCM removed under reduced pressure. This mesylate salt (complex **7**) was then dissolved in a THF (10 mL)/EtOH (3 mL) mixture and degassed with sonication for 30 min. The solution was brought to reflux under  $N_2$  in the dark. Thiourea (30 mg, excess) was added and the reflux continued for a further 8 h.  $N_2$  gas was then flushed through the reaction mixture, degassed aqueous NaOH (20%, 6 mL, 30 min sonication) was added and the reflux continued for a further 2 h.

This mixture was subsequently poured into a dilute HCl/ice mixture, extracted with DCM (2 × 40 mL) and dried over  $MgSO_4$ , filtered and the solvent evaporated. The final phthalocyanine complex **8** was then purified twice with BioBeads using DCM as the eluent. Yield: 12%. UV/vis (DMSO):  $\lambda_{max}$  nm (log  $\epsilon$ ): 706 (4.64), 638 (4.08), 364 (4.33). IR (KBr):  $\nu_{max}/cm^{-1}$ : 2997 (C–H), 1436, 1406 (C=C), 1307 (C–H), 667 (C–S–C).  $^1H$  NMR (600 MHz, DMSO- $d_6$ )  $\delta$  (ppm): 7.70–7.69 (dd, 4H, Ar–H), 7.53–7.51 (dd, 4H, Ar–H), 6.97 (s, 4H, Ar–H), 4.22 (m, 8H, CH<sub>2</sub>–S–Ar), 1.67 (m, 8H, CH<sub>2</sub>–S), 1.43–1.24 (m, 32H, CH<sub>2</sub>). SH protons not observed. Calc. for  $C_{56}H_{64}N_8S_8Zn$ : C; 57.38, H; 5.59, N; 9.56, Found: C; 57.35, H; 5.44, N; 9.65. MALDI-TOF-MS  $m/z$ : Calc: 1171.08; Found [M]<sup>+</sup>: 1170.56.

**[8,15,22-Tris-(naphtho)-2-(amidoethanethiol)phthalocyanato] zinc(II) (10 Scheme 3).** Under an Ar atmosphere, complex **9** (2 mg, 2  $\mu$ mol) and DCC (0.4 mg, 2  $\mu$ mol) were dissolved in a mixture of dry DMSO (2 mL) and pyridine (0.8 mL). After 10 min of stirring at 0 °C, cysteamine was added to the mixture and the reaction was left to stir at room temperature for 48 h. The product was purified using column chromatography on BioBeads. THF was used as an eluent. Yield: ~10%. UV-vis (THF):  $\lambda_{max}$  nm (log  $\epsilon$ ): 733 (4.57), 687 (4.31), 655 (4.03), 615 (3.86), 353 (4.27). IR  $\nu_{max}/cm^{-1}$ : 3000 (amide N–H), 2562 (S–H), 1693 (C=O coupled to N–H), 1323 (Aryl NH). Calc. for:  $C_{65}H_{39}N_9SO_4Zn$ : C, 70.49; H, 3.55; N, 11.36; S, 2.89%; found C, 69.97; H, 3.81; N, 11.77; S,

2.66.  $^1H$  NMR (600 MHz,  $CDCl_3$ )  $\delta$  (ppm): 8.20–6.72 (m, 34H, Ar–H, N–H), 1.50–0.82 (m, 4H, methylene). MALDI-TOF-MS  $m/z$  Calc: 1107.51; found (M–H)<sup>+</sup>: 1108.24.

**Gold nanoparticles (TOABr–AuNP).** The gold nanoparticles were synthesized according to a procedure previously reported in literature.<sup>25,39</sup> Briefly, a gold solution was prepared by stirring  $HAuCl_4 \cdot 3(H_2O)_3$  (0.019 g, 25 mM) in toluene (2 mL). A solution of TOABr (0.139 g, 85 mM) in 3 mL toluene was added to the gold solution and the mixture was vigorously stirred until the colour of the mixture changed from yellow to a brownish-yellow colour. Thereafter  $NaBH_4$  (0.002 g, 36 mM) in 2 mL of water was added dropwise to the gold solution until the solution changed colour from brownish-yellow to milky then scarlet and finally to a purple colour. The mixture was left to stir for a further 30 min. The gold nanoparticles were washed repeatedly with water to remove the reducing agent and were stored in a minimum amount of toluene. The concentration of the TOABr–AuNPs was estimated to be  $4.99 \times 10^{-5} M^{-1} L^{-1}$ . After a couple of days the solution turned colourless and additional amounts of  $NaBH_4$  (36 mM, in water) was added to refurbish the nanoparticles.

**Self assembly of phthalocyanines onto gold nanoparticles (Scheme 3).** In 1 mL THF or chloroform, complexes **3**, **8** or **10** (1  $\mu$ M) and TOABr–AuNP (0.5  $\mu$ L in toluene) were stirred at room temperature for 48 h under Ar atmosphere and protection from light. Purification of the Pc–AuNP conjugates was performed using column chromatography on Bio-Beads with THF or chloroform as the eluting solvent.

### Photophysical properties

**Fluorescence quantum yields and lifetimes.** The comparative method was used to determine the fluorescence quantum yields ( $\Phi_F$ ) of the phthalocyanine complexes using eqn (2).<sup>42</sup>

$$\Phi_F = \Phi_{F(Std)} \frac{FA_{Std}n^2}{F_{Std}An_{Std}^2} \quad (2)$$

where  $F$  and  $F_{Std}$  are the areas under the fluorescence curves of the complexes (**3**, **8** and **10** and their AuNP conjugates) and the standard respectively.  $A$  and  $A_{Std}$  are the respective absorbances of the sample and the standard at the excitation wavelength and  $n$  and  $n_{Std}$  are the refractive indices of the solvents used for the sample and standard respectively. ZnPc was used as a standard in DMSO where  $\Phi_F = 0.20$ .<sup>43</sup>

**Triplet quantum yields and lifetimes.** The triplet quantum yields were determined using eqn (3):<sup>44</sup>

$$\Phi_T = \Phi_T^{Std} \frac{\Delta A_T \epsilon_T^{Std}}{\Delta A_T^{Std} \epsilon_T} \quad (3)$$

where  $\Delta A_T$  and  $\Delta A_T^{Std}$  are the changes in the triplet state absorbances of complexes **3**, **8** or **10** and the standard, respectively.  $\epsilon_T$  and  $\epsilon_T^{Std}$  are the triplet state molar extinction coefficients for complexes **3**, **8** or **10** (and their conjugates) and the standard, respectively.  $\Phi_T^{Std}$  is the triplet quantum yield for the standard, ZnPc ( $\Phi_T^{Std} = 0.58$  in DMF).<sup>45</sup> Triplet lifetimes were determined by exponential fitting of the kinetic curves using OriginPro 8 software.

## Conclusions

The synthesis and characterization of 9,16,23-tris-(5-trifluoromethyl-2-mercaptopyridine)-2-(carboxy)phthalocyanine (**3**), 2,9,17,23-tetrakis-[(1, 6-hexanedithiol)phthalocyaninato] zinc(II) (**8**) and [8,15,22-tris-(naphtho)-2-(amidoethanethiol)phthalocyaninato] zinc(II) (**10**) was successfully achieved. Gold nanoparticles were synthesized, characterized and linked to phthalocyanines. Low fluorescence quantum yields, high triplet quantum yields and low triplet lifetimes were observed for the conjugates, compared to free Pc complexes with the exception of **8** for  $\Phi_T$ . Fluorescence lifetimes indicate bi-exponential decay kinetics for **3-AuNP** and **10-AuNP** where the much smaller second lifetime was attributed to the linked species. However, the **8-AuNP** conjugate showed a mono-exponential decay indicating that the presence of four SH groups at the terminal end of the Pc results in strong binding to the AuNP leading to non-fluorescent phthalocyanines.

## Acknowledgements

This work was supported by the Department of Science and Technology (DST) and National Research Foundation (NRF), South Africa through DST/NRF South African Research Chairs Initiative for Professor of Medicinal Chemistry and Nanotechnology as well as Rhodes University and Medical Research Council of South Africa.

## Notes and references

- R. Bonnett, in *Chemical Aspects of Photodynamic Therapy*, Gordon and Breach Science Publishers, Amsterdam, 2000.
- R. K. Panday, *J. Porphyrins Phthalocyanines*, 2000, **4**, 368.
- I. Rosenthal, *Photochem. Photobiol.*, 1991, **53**, 859.
- T. K. Lee, E. D. Baron and T. H. Foster, *J. Biomed. Opt.*, 2008, **13**, 030507.
- T. J. Dougherty, C. J. Gomer, B. W. Henderson, G. Jori, D. Kessel, M. Korbek, J. Moan and Q. Peng, *J. Natl. Cancer Inst.*, 1998, **90**, 889.
- A. P. Castano, T. N. Demidova and M. R. Hamblin, *Photodiagn. Photodyn. Ther.*, 2005, **2**, 1.
- J. Usuda, S. M. Chiu, E. S. Murphy, M. Lam, A. L. Nieminen and N. L. Oleinick, *J. Biol. Chem.*, 2003, **278**, 2021.
- S. E. Choi, S. Sohn, J. W. Cho, E. A. Shin, P. S. Song and Y. Kang, *J. Photochem. Photobiol., B*, 2004, **73**, 101.
- S. L. Haywood-Small, D. I. Vernon, J. Griffiths, J. Schofield and S. B. Brown, *Biochem. Biophys. Res. Commun.*, 2006, **339**, 569.
- K. Berg, P. K. Selbo, A. Weyergang, A. Dietze, L. Prasmickaite, A. Bonsted, B. Ø. Engesaeter, E. Angellpetersen, T. Warloe, N. Frandsen and A. Hogset, *J. Microsc.*, 2005, **218**, 133.
- D. A. Giljoham and C. A. Mirkin, *Nature*, 2009, **462**, 461.
- S. Bhattacharyya, R. A. Kudgus, R. Bhattacharyya and P. Mukherjee, *Pharm. Res.*, 2011, **28**, 237.
- M. C. Daniel and D. Astruc, *Chem. Rev.*, 2004, **104**, 293.
- Z. Tang and N. A. Kotov, *Adv. Mater.*, 2005, **17**, 951.
- B. Duncan, C. Kim and V. M. Rotello, *J. Controlled Release*, 2010, **148**, 122.
- P. K. Jain, I. H. El-Sayed and M. A. El-Sayed, *Nano Today*, 2007, **2**, 18.
- Y. D. Cheng, J. D. Meyers, A. M. Broome, M. E. Kenney, J. P. Basilion and C. Burda, *J. Am. Chem. Soc.*, 2011, **133**, 2583.
- Y. Cheng, A. C. Samia, J. Li, M. E. Kenney, A. Resnick and C. Burda, *Langmuir*, 2010, **26**, 2248.
- M. E. Wieder, D. C. Hone, M. J. Cook, M. M. Handsley, J. Gavriloic and D. A. Russell, *Photochem. Photobiol. Sci.*, 2006, **5**, 727.
- C. M. Goodman, C. D. McCusker, T. Yilmaz and V. M. Rotello, *Bioconjugate Chem.*, 2004, **15**, 897.
- C. J. Murphy, A. M. Gole, J. W. Stone, P. N. Sisco, A. M. Alkilany, E. C. Goldsmith and S. C. Baxter, *Acc. Chem. Res.*, 2008, **41**, 1721.
- M. Camerin, M. Magaraggia, M. Soncin, G. Jori, G. M. Moreno, I. Chambrier, M. J. Cook and D. A. Russell, *Eur. J. Cancer*, 2010, **46**, 1910.
- D. C. Hone, P. I. Walker, R. Evans-Gowing, S. FitzGerald, A. Beeby, I. Chambrier, M. J. Cook and D. A. Russell, *Langmuir*, 2002, **18**, 2985.
- A. Kotiaho, R. Lahtinen, A. Efimov, H. K. Metsberg, E. Sariola, H. Lehtivuori, N. V. Tkachenko and H. Lemmetyinen, *J. Phys. Chem. C*, 2010, **114**, 162.
- M. G. Debacker, O. Deleplanque, B. Van Vlieberge and F. X. Sauvage, *Laser Chem.*, 1988, **8**, 1.
- N. Nombona, E. Antunes and T. Nyokong, *Dyes Pigm.*, 2010, **86**, 68.
- J. G. Young and W. Onyebuagu, *J. Org. Chem.*, 1990, **55**, 2155.
- N. Masilela and T. Nyokong, *Dyes Pigm.*, 2011, **91**, 164.
- A. Erdogmus, S. Moeno, C. Litwinski and T. Nyokong, *J. Photochem. Photobiol., A*, 2010, **210**, 200.
- N. Nombona, W. Chidawanyika and T. Nyokong, *Polyhedron*, 2011, **30**, 654.
- M. J. Stillman and T. Nyokong, in *Phthalocyanines-Properties and Applications*, ed. A. B. P. Lever and C. C. Leznoff, VCH, New York, 1989.
- M. Durmuş and T. Nyokong, *Spectrochim. Acta, Part A*, 2008, **69**, 1170.
- S. Sapra and D. D. Sarma, *Pramana*, 2005, **65**, 565.
- F. Mafune, *Chem. Phys. Lett.*, 2004, **397**, 133.
- K. G. Thomas and P. V. Kamat, *Acc. Chem. Res.*, 2003, **36**, 888.
- W. Freye, S. Mueller and K. J. Teuchner, *J. Photochem. Photobiol., A*, 2004, **163**, 231.
- J. R. Lakowicz, *Anal. Biochem.*, 2005, **337**, 171.
- E. Dulkeith, M. Ringler, T. A. Klar, J. Feldmann, A. M. Javier and W. J. Parak, *Nano Lett.*, 2005, **5**, 585.
- M. Brust, M. Walker, D. Bethel, D. J. Schiffrin and R. Whyman, *J. Chem. Soc., Chem. Commun.*, 1994, 801.
- J. R. Lakowicz, in *Principles of Fluorescence Spectroscopy*, Kluwer Academic/Plenum Publishers, New York, 1999.
- I. Chambrier, M. J. Cook and D. A. Russell, *Synthesis*, 1995, 1283.
- S. Fery-Forgues and D. Lavabre, *J. Chem. Educ.*, 1999, **76**, 1260.
- A. Ogunsipe, J. Y. Chen and T. Nyokong, *New J. Chem.*, 2004, **28**, 822.
- T. H. Tran-Thi, C. Desforge and C. Thiec, *J. Phys. Chem.*, 1989, **93**, 1226.
- J. Kossanyi and O. Chahraoui, *Int. J. Photoenergy*, 2000, **2**, 9.